# Coupling of ultrafast laser energy to coherent phonons in bismuth

Alexander Q. Wu and Xianfan Xu

Citation: Applied Physics Letters **90**, 251111 (2007); doi: 10.1063/1.2750401
View online: http://dx.doi.org/10.1063/1.2750401
View Table of Contents: http://scitation.aip.org/content/aip/journal/apl/90/25?ver=pdfcov
Published by the AIP Publishing

# Development of a Quantum-Voltage-Calibrated Noise Thermometer at NIM

J. Qu[1], J. T. Zhang[1], Y. Fu[1],
H. Rogalla[2], A. Pollarolo[2], and S. P. Benz[2]

[1] *National Institute of Metrology, Beijing 100013, P. R. China*
[2] *National Institute of Standards and Technology, Boulder, CO 80305, USA*

**Abstract.** A quantum-voltage-calibrated Johnson-noise thermometer was developed at NIM, which measures the Boltzmann constant $k$ by comparing the thermal noise across a 100 Ω sense resistor at the temperature of the triple point of water with the pseudo-random frequency-comb voltage waveform synthesized with a bipolar-pulse-driven quantum-voltage-noise source. A measurement with integration period of 10 hours and bandwidth of 640 kHz resulted in a relative offset of $0.5\times10^{-6}$ from the current CODATA value of $k$, and a type A relative standard uncertainty of $23\times10^{-6}$. Benefiting from closely matched noise powers and transmission-line impedances and small nonlinearities in the cross-correlation electronics, the derived $k$ shows self-consistent values and standard uncertainties for different measurement bandwidths.

**Keywords:** Boltzmann constant, Correlation, Josephson junction arrays, Noise, Quantization, Thermometry.

## INTRODUCTION

There has been much interest in developing different methods to measure the Boltzmann constant $k$ at an uncertainty level comparable to that of acoustic-gas-based thermometry, which dominates the current CODATA value of $k$ [1-2]. The Johnson noise thermometer (JNT) measures the thermodynamic temperature $T$ through the Nyquist relation $\langle V^2\rangle = 4kTR\Delta f$, by measuring the voltage noise power $\langle V^2\rangle$ arising from the thermal fluctuation of the electrons in a resistor $R$ over a frequency bandwidth $\Delta f$ [3]. Alternatively, by measuring $\langle V^2\rangle$ across $R$ at a known $T$, the JNT provides the possibility to determine $k$. However, the challenge is that it is difficult to measure the thermal noise with small statistical uncertainty [4].

Recently, NIST reported the measurement of $k$ with JNT through comparing the thermal noise spectrum of a 100 Ω resistor at the triple point water (TPW) temperature to the calculable pseudo-noise voltage waveform synthesized by a quantized voltage noise source (QVNS) [5]. Though the measured value of $k$ is consistent with the CODATA 2010 value, the $12\times10^{-6}$ relative uncertainty of the measurement is one order of magnitude higher than the $1.2\times10^{-6}$ relative uncertainty of the acoustic-gas-thermometry measurement [6], and the $9.1\times10^{-7}$ relative uncertainty of the current CODATA value [1]. The uncertainty of the NIST QVNS-JNT measurement is dominated by (1) the aberrations in the power-ratio spectra produced by systematic errors ($10.4\times10^{-6}$), and (2) the random statistical uncertainty ($5\times10^{-6}$) [5]. Neither the systematic errors nor the statistical uncertainty is currently believed to represent a fundamental limit on this electronic measurement.

In order to demonstrate the reproducibility of this electrical approach to measuring $k$, and to determine the sources of systematic errors to pursue lower measurement uncertainty comparable to the acoustic-gas-based thermometry, it is important to develop another QVNS-JNT system and perform independent measurements. With a NIST-fabricated Josephson-junction array chip, we developed a new QVNS-JNT system at NIM that is different from the NIST system in some aspects. In this paper, we describe the construction of the NIM system and report our first measurement result that shows improvement in the frequency response compared to the previous measurement result with the NIST system.

## SYSTEM CONSTRUCTION

Figure 1 shows the schematic of the NIM QVNS-JNT system. Both the QVNS and the sense resistor (R) are equally divided by a center tap that is connected to ground to provide differential noise signals. A switch circuit switches the QVNS or R to the two nominally identical amplification channels. Each amplification channel contains a low-noise high-gain differential preamplifier (Preamp), a low-pass filter (LPF), a

*Temperature: Its Measurement and Control in Science and Industry, Volume 8*
AIP Conf. Proc. 1552, 29-33 (2013); doi: 10.1063/1.4821369

buffer amplifier (Buffer), and an analog-to-digital converter (ADC) within which an anti-aliasing filter is integrated. The digitized signals are transferred to computer via optical fibers and cross-correlated by software. All the electronics are sealed in aluminum boxes and powered by batteries. In the following paragraphs, we describe the signal processing blocks in more detail.

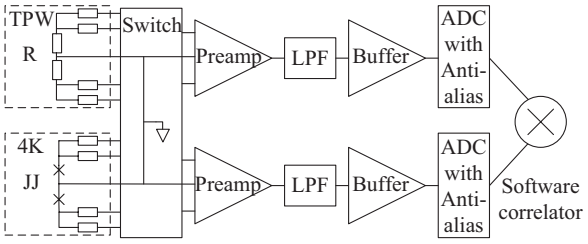


**FIGURE 1.** Schematic of the NIM QVNS-JNT system.

The photographs of the sense resistor and the thermometer probe are shown in Fig. 2. The custom sense resistor R consists of two Ni–Cr-alloy foils on an alumina substrate with nominal resistance value of 50 Ω for each. Two pairs of gold-coated leads on the hermetically sealed package are connected to the two ends of the resistor network and a fifth lead is connected to the center. The resistor package is mounted on a copper header soldered at the bottom end of a thin-wall stainless steel probe. The probe is about 60 cm long and vacuum sealed. Two cables with the same length made of three Teflon-insulated wires transmit the differential noise signals from the resistor to the connectors at the top of the probe. The probe is immersed in a glass cell that maintains the temperature of the TPW. The cell is placed in a stainless steel dewar filled with ice, instead of a thermal electrical cooler, to minimize electromagnetic interference (EMI). The resistance of the sensor is measured by a DC resistance bridge to be 100.0065 Ω.

The QVNS chip was fabricated at NIST in Boulder. There are 10 superconductor-normal metal-superconductor (SNS) Josephson junctions in each of two arrays [7]. The chip is mounted on a flexible package in a magnetically shielded probe. The probe is cooled to 4 K in a 100 l liquid-helium Dewar. The critical current of the Josephson junctions is around 6 mA and the characteristic frequency is about 5 GHz. The quantum-voltage-noise waveform is synthesized by the bipolar pulse-driven technique. Though the operation margin of the Josephson junction array is lower than that for the unipolar pulse-driven synthesis [7], the advantage is that there is no DC offset for the synthesized AC waveform. The frequency of the microwave signal that drives the pulse generator is 9.999 872 GHz, which is split by the pulse generator to get the sampling frequency $f_s$ = 4.999 936 GHz. The bit length of the digital code is selected to be $M$ = 4 999 936, so that the repetition frequency of the waveform is $f_1 = f_s/M$ = 1 kHz. The comb-like multi-tone waveform consists of odd harmonic tones of $f_1$ from 1 kHz to 999 kHz with tone spacing of 2 kHz. The tone amplitude is set to 54.9268 nV to ensure the voltage spectral density $V_Q$ = 1.2282 nV/Hz$^{1/2}$ closely matches the spectral density of the thermal noise, $V_R$ = 1.228272 nV/Hz$^{1/2}$, of the 100.0065 Ω resistor at the TPW.

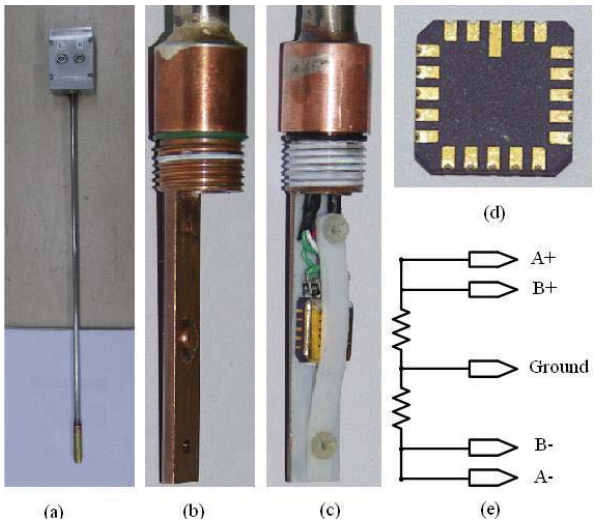


**FIGURE 2.** Photographs of the (a) resistor probe, (b) copper header of the probe, (c) copper head with the sense resistor mounted, (d) sense resistor chip package, and (e) schematic of the sense resistor circuit.

Note that four resistors with nominal resistance of 100 Ω are fabricated in the superconducting wires on the Josephson junction chip to match the resistance of the sense noise source. These resistors introduce extra uncorrelated noise at 4 K. Additional small chip resistors of 1.5 Ω are inserted between the signal leads and the transmission wires for both the QVNS and R to more closely match the uncorrelated noise power and resistance.

The switch circuit consists of four latching relays mounted on a FR4 printed circuit board (PCB). The relays are controlled by a field programmable gate array (FPGA) to alternate between the noise sources such that either the QVNS or the resistor is connected to the two cross-correlation channels. In the PCB, the signal traces are symmetrically placed in the top layer and the total length from input lead to output lead is about 15 mm. The copper ground plane is in the bottom layer, in which the area opposite to the signal

traces is removed. This is important because the smallest possible shunt capacitance helps to minimize the effect of dielectric losses [5].

The preamplifier plays the most important role in the cross-correlation electronics. In our system, the preamplifier is of similar design to that in the NIST system [8], and has a gain of $70 \pm 0.5$ dB and noise floor of 1.2 nV/Hz$^{1/2}$ in the DC -to-1 MHz bandwidth and a common-mode-rejection-ratio of 100 dB at 100 kHz. Due to a lack of the low-noise JFETs, the mirror current source uses a pair of low-noise transistors.

The nonlinearity of the preamplifier was demonstrated to significantly affect the performance of the QVNS-JNT system. Previous NIST measurements used odd multi-tone voltage waveforms with increasing density and decreasing amplitude of the tones to reduce the effect of nonlinearities [8]. With further investigation, it was found that the DC offset of the signal before the differential stage of the preamplifier was the main source of the distortion [9]. In the present preamplifier, an offset compensation circuit is included to nulls the DC offset of the signal before the differential stage.

Two-tone waveforms were synthesized by the QVNS to measure the distortion arising from the remaining nonlinearity. Figure 3 shows the auto- and cross-correlation measurements of a synthesized waveform with two tones at 300 kHz and 301 kHz with 8 μV rms amplitudes. The different distortion products are represented with different symbols. The third-order inter-modulation (IM) distortion is hidden by the cross-correlation noise floor. The amplitudes for the second order IM and harmonic distortion tones are 0.7 nV and 0.35 nV, respectively. Note that in the present measurement, the tone amplitude of the input signal is twice of that in Fig. 6 of [8], while the second order distortion is lower. By extrapolating the amplitude dependence of the distortion on the input signals (not shown here), we found that for waveforms with a tone amplitude of 54.9268 nV, the second order IM distortion is -121.5 dBc, and the others are even lower.

The amplified signal in each channel is filtered by the 11-pole LPF with cut-off frequency of 800 kHz, which defines the measurement bandwidth, and then is amplified by the Buffer with gain of 5.5×, which in turn drives the ADC.

Commercial ADCs with high resolution of 20 bits at 2 MHz sampling frequency are used for data acquisition. There is a 1 MHz anti-aliasing filter integrated within the ADC to prevent the aliased high-frequency signals from contributing to the measured noise-power spectra. The ADCs are clocked and triggered by external clocks provided by commercial function generators via optical fibers. The phases of the clocks are adjusted carefully before the measurement so that the phase difference between the two acquisitions is less than 10 ps.

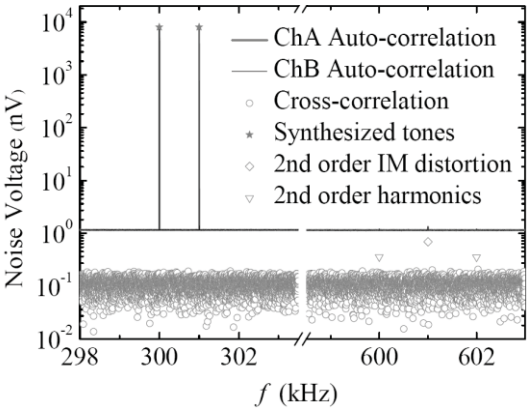


**FIGURE 3.** Auto- and cross-correlation power spectral density of a QVNS-synthesized two-tone waveform. Second-order IM distortion harmonics are indicated with different symbols.

The data are then optically transmitted to the computer. The software correlator cross-correlates the data that are acquired for every 1 s, accumulates these data for 100 s and saves the result, and then switches the relays to measure the other noise source.

People might be interested in the differences of the present NIM system from the one at NIST. In Table 1, we summarize the main differences between the two systems, where the points regarding to the NIM system have been described in the above paragraphs. One can learn more details of the NIST system elsewhere [5, 7-9].

**TABLE 1.** The main differences between the NIM and NIST systems.

| | NIM system | NIST system |
|---|---|---|
| QVNS pulse bias | bipolar (no dc offset voltage) | unipolar (small dc offset voltage) |
| TPW temperature control | ice bath | thermo-electric cooler |
| switching circuit | 1 relay connection from input to output | 2 relay connections from input to output |
| Amplifier | 1.2 nV/Hz$^{1/2}$ noise floor | 0.85 nV/Hz$^{1/2}$ noise floor |
| Filtering | 800 kHz LPF and 1 MHz anti-aliasing | 650 kHz LPF and 800 kHz LPF |
| ADC | commercial, 20 bit, 2 MHz sampling | custom, 16 bit, 2.08 MHz sampling |

## MEASUREMENT RESULT

Keeping the environment electrically quiet is important to get a reliable measurement result. Generally, we run the measurement at night for about 10 hours. The averaged auto- and cross-correlation power spectra of the thermal and electrical noise, denoted as $\langle S_R \rangle$ and $\langle S_Q \rangle$ respectively, were summed and compared over discrete 2 kHz intervals centered at the frequency of the tones of the QVNS synthesized waveform. The noise power ratio $\langle S_R \rangle / \langle S_Q \rangle$ is expected to be close to unity and show flat frequency response. However, because different transmission lines are used to transmit the noise signals from the sense resistor and QVNS to the amplifiers, different transfer functions may occur and result in the deviation of the noise-power ratio from unity. It is very important to match both the noise power and the transmission-line impedance to minimize the deviation and, hence, the effects of nonlinearities. In our measurement, close matching is achieved by carefully trimming the value of the resistors inserted in the sense resistor and QVNS transmission lines, as well as the length of the lines.

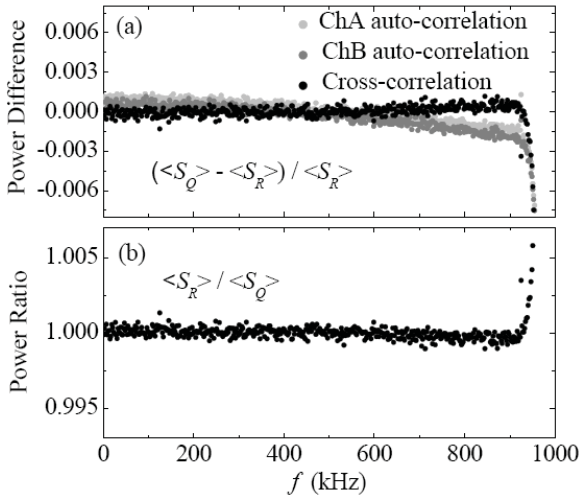


**FIGURE 4.** (a) Differences of the auto- and cross-correlated noise-power spectra between the electrical and thermal noise, and (b) ratio of the noise-power spectra.

Figure 4(a) shows the relative difference of the auto- and cross-correlated noise power spectra between the QVNS and the sense resistor for a 10 h measurement. It can be seen that the two auto-correlation differences are matched to better than 2 parts in $10^3$, and show a weak quadratic dependence with frequency. The cross-correlation noise is matched to better than 1 part in $10^3$. Figure 4(b) presents the ratio of the thermal and electrical noise powers. The $\langle S_R \rangle / \langle S_Q \rangle$ shows almost flat frequency response and very small remaining quadratic behavior.

The remaining quadratic frequency dependence of the noise-power ratio can be corrected by least-squares fitting the data with a two-parameter formula $a_0+a_2f^2$. The fitting coefficient $a_0$ and associated standard deviation are used to determine $k$ and its relative statistical uncertainty. The coefficient $a_2$ characterizes the remaining quadratic response.

The variation with increasing integration period of the fitting parameter $a_0$ and its standard deviation $\sigma$ are tracked and plotted in Fig. 5, for a fitting bandwidth of 640 kHz. The difference $a_0$-$a_0^{2010}$ represents the relative offset of $k$ from the 2010 CODATA value and $a_0^{2010} = (V_R/V_Q)^2$, and the chop number $N$ indicates the integration period where one chop corresponds to the two consecutive accumulations of both the thermal and electrical noise signals for 100 s each. One can see from Fig. 5(a) that the relative offset of $k$ fluctuates around zero and tends to be flat with increasing chop number. In Fig. 5(b), the relative statistical uncertainty determined from the standard deviation of $a_0$ decreases linearly with increasing chop number on a logarithmic scale. Indeed, it closely follows the straight line that represents the theoretically expected $1/N^{1/2}$ behavior of the statistical uncertainty [10]. By averaging all the data for the 182 chops, the relative offset of $k$ is found to be $0.5\times10^{-6}$ and the relative statistical uncertainty approaches $23\times10^{-6}$.

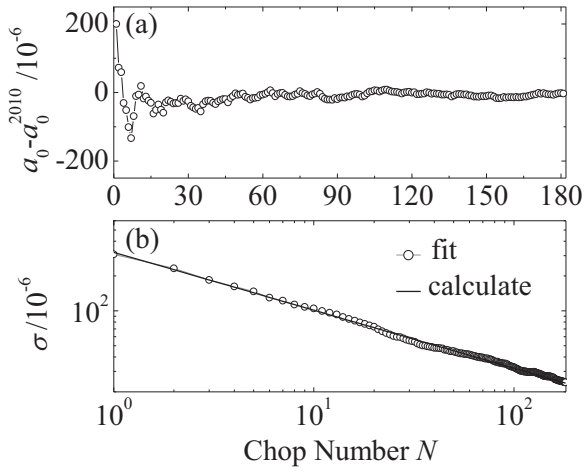


**FIGURE 5.** Variations of (a) the fitting parameter $a_0$, and (b) its standard deviation $\sigma$ with increasing integration period for a fitting bandwidth of 640 kHz. The straight line in (b) represents the theoretically expected statistical uncertainty [10].

For the previous QVNS-JNT measurement with the NIST system, small spectral aberrations were found for the variation of $a_0$ when the data were fitted over

different bandwidths. The aberrations are probably caused by systematic errors and they dominated the measurement uncertainty [5]. To check the present measurement, the resulting difference $a_0$-$a_0^{2010}$ and associated statistical measurement uncertainties, from fitting the data with different bandwidths starting from 5 kHz and ending at successively higher frequencies, are plotted in Fig. 6. It is important to note that $a_0$ shows flat behavior as a function of fit bandwidth. The values of $a_0$-$a_0^{2010}$ are consistent with each other within the error bars for the standard deviations of the different fitting bandwidths. The flat result demonstrates the self-consistency of the data, and indicates that the systematic error that produced the spectral aberrations in the previous measurement with the NIST system is greatly reduced.

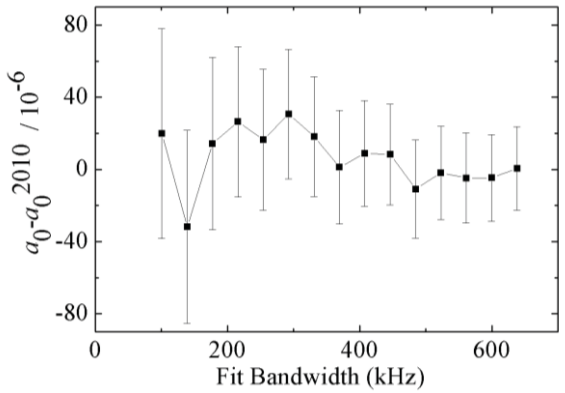


**FIGURE 6.** Self-consistency of the fitting parameters $a_0$ for different fitting bandwidths.

## CONCULSION

A QVNS-JNT system was developed at NIM to demonstrate reproducibility and pursue lower uncertainty for the electronic measurement of the Boltzmann constant. The system consists of closely matched QVNS and sense resistor noise sources, a custom switch circuit with perfectly symmetric signal traces, low-noise high-gain preamplifiers with small nonlinearities, and high-speed ADCs with high resolution. The quadratic fitting parameters of the measured power ratio showed extremely flat dependence on the different fitting bandwidth, indicating that the systematic errors that produced the spectral aberrations in the NIST system are greatly reduced. A measurement with an integration period of 10 hours resulted in a relative offset of $0.5\times10^{-6}$ from the CODATA 2010 value of $k$, and a type A statistical uncertainty of $23\times10^{-6}$. Further improvements are under way to reach the goal of an electronic measurement of $k$ at a combined relative uncertainty less than $10\times10^{-6}$.

## ACKNOWLEDGEMENTS

We thank Paul Dresselhaus and Charlie Burroughs for chip fabrication and packaging, and D. Rod White, Weston L. Tew, Kazuaki Yamazawa and Chiharu Urano for helpful discussions. The work is supported by NSFC and the public welfare scientific research project.

## REFERENCES

1. Mohr, P. J., Taylor, B. N., and Newell, D. B., *Rev. of Mod. Phys.*, to be published, (2012).
2. Fischer, J., and Fellmuth, B., *Int. J. Thermophys.* **28**, 1753–1765, (2008).
3. Nyquist, H., *Phys. Rev.* **32**, 110–113 (1928).
4. White, D. R., Galleano, R., Actis, A., Brixy, H., Groot, M., Dubbeldam, J., Reesink, A. L., Edler, F., Sakurai, H., Shepard, R. L., and Gallop, J. C., *Metrologia* **33**, 325–335 (1996).
5. Benz, S. P., Pollarolo, A., Qu, J. F., Rogalla, H., Urano, C., Tew, W. L., Dresselhaus, P. D., and White, D. R., *Metrologia*, **48**, 142-153 (2011).
6. Pitre, L., Sparasci, F., Truong, D., Guillou, A., Risegari, L., and Himbert, M. E., *Int. J. Thermophys.*, **32**, 1825-1886, (2011).
7. Benz, S. P., Dresselhaus, P. D. and Burroughs, C. J., *IEEE Trans. Appl. Superc.*, **21**, 681-686 (2011).
8. Qu, J. F., Benz, S. P., Rogalla, H., and White, D. R., *Metrologia*, **46**, 512-524 (2009).
9. Qu, J. F., Benz, S. P., Pollarolo, A., Rogalla, H., *IEEE Trans. Instrum. Meas.,* **60**, 2427-2433 (2011).
10. White, D. R., Benz, S. P., Labenski, J. R., Nam, S. W., Qu, J. F., Rogalla, H., and Tew, W. L., *Metrologia*, **45**, 495-305 (2008).